Highlights

Measurement of polarization in Lyman-α line caused by anisotropic electron collisions in LHD plasma

N. Ramaiya, M. Goto, G. Seguineaud, T. Oishi, S. Morita

- Lyman-α line coming from the edge LHD plasma is polarized
- Polarization degree of the order of 0.03 has been clearly observed
- Polarization direction is found to be related to the magnetic field direction
- Anisotropic electron velocity distribution function at inboard side causes polarization

Measurement of polarization in Lyman-α line caused by anisotropic electron collisions in LHD plasma

N. Ramaiya[a,*], M. Goto[a,b], G. Seguineaud[a], T. Oishi[a,b], S. Morita[a,b]

[a] *Department of Fusion Science, The Graduate University for Advanced Studies, SOKENDAI, Toki 509-5292, Japan*
[b] *National Institute for Fusion Science, Toki 509-5292, Japan*

Abstract

Polarization in the Lyman-α line caused by anisotropic electron collisions has been investigated in the Large Helical Device (LHD). High-sensitivity polarization-resolved measurements of the Lyman-α line from edge LHD plasma have been carried out. To obtain spectra of linearly polarized light at all angles a high-reflectivity mirror, a polarization analyzer, and a half-waveplate have been additionally installed into an existing VUV spectrometer system. These optical components have been designed and developed by the CLASP (Chromospheric Lyman-Alpha Spectro-Polarimeter) [R Kano et al. ApJL, 839(1):L10, 2017] team. The present measurement has been made during an electron cyclotron heated discharge. Intensity of the Lyman-α line integrated over line profile has been obtained and plotted as a function of time to generate temporal profile of line. The profile shows that intensity of light varies in synchronization with the angle of the observed linearly polarized light, which clearly indicates that the line is polarized. By performing

*Corresponding author
Present address: Institute for Plasma Research, Gandhinagar-382428, India
Email address: nilam.ramaiya@gmail.com (N. Ramaiya)

least-squares fitting on the temporal profile, the magnitude of polarization degree has been evaluated to be 0.033 ± 0.004. In addition, phase analysis of the measured intensity variation has been carried out. From this analysis it has been found that the observed polarization in Lyman-α can be attributed to the anisotropic electron velocity distribution function (EVDF) at the inboard side of LHD plasma. The preliminary results of a simulation model code suggest that the value of polarization degree is negative and electron temperature in the perpendicular direction to the magnetic field is higher compared to electron temperature in the parallel direction. Therefore, the final value of polarization degree in Lyman-α is -0.033 ± 0.004.
Keywords: polarization, Lyman-α line, anisotropy, electron cyclotron heating, VUV spectrometer, half-waveplate, Brewster's angle

1. Introduction

The electron velocity distribution function (EVDF) in a plasma is one of the most important attributes of the plasma. In a magnetically confined plasma EVDF may show some anisotropy. For clear understanding of plasma confinement and transport phenomena in a plasma, the measurement of anisotropy in EVDF is indispensable. Although the anisotropic EVDF plays a key role in a magnetically confined fusion plasma, there is a lack of studies that actively investigate EVDF in plasma experiments.

Over the years several diagnostics techniques, for example, electrical probes [1, 2], a directional velocity analyzer [3], Thomson scattering [4, 5], absorption of waves [6, 7] and polarization in emission lines of atoms or ions [8] have been developed to study the anisotropic EVDF. The experimental

studies show that the presence of high-energy electrons can cause significant errors in measurements carried out using electrical probes, which limits the use of electrical probes in a burning plasma device. Thomson scattering diagnostic is quite reliable system but it requires very powerful and fast lasers, large collection optics, and sensitive background subtraction techniques must be used. Such a system presents tremendous integration and operational issues in a fusion grade plasma device. In addition, the lasers and optical components have limited lifetime. Steady-state operation would also put significant constraints on the laser system, by rapidly exceeding their lifetimes. The techniques based on absorption of waves make use of wave absorption due to a Doppler-shifted cyclotron resonance with electrons. Operation at GHz frequencies presents many challenges. It is very difficult to acquire data with a high enough time resolution for direct measurement of waves with GHz frequencies. Impedance matching at connections between coaxial cables and other components in an experimental circuit is very crucial as a slight impedance mismatching causes signal reflections, which affects the accuracy of measurement.

From electron beam impact experiments and theoretical calculations it is well known that anisotropic electron-impact excitation creates non-uniform population distribution over the magnetic sublevels in a state and subsequent emission is polarized. Therefore, polarization spectroscopy is a useful technique to study anisotropy in the EVDF. Compared to diagnostic techniques like Thomson scattering and absorption of waves, the technique of polarization spectroscopy has several advantages. The major components used in the system for acquiring polarization measurements are a spectrometer with a

CCD (Charge Coupled Device) detector and some additional optical components like a half-waveplate and a mirror. The arrangement of optical components inside the system is very simple and also integration of the system on a device and its operation is not complicated. Due to longer lifetimes of spectrometers and CCD detectors, this technique is suitable for steady-state operations also. In addition, data acquisition time for polarization measurements can be decided depending on a discharge conditions, and very high time resolution is not required. In the present study, we address the polarization in Lyman-α line caused by anisotropic collisions with electrons.

Spectral profiles of a hydrogen line from the LHD plasma have been studied earlier and emission locations were identified on the magnetic field map [9, 10]. The results indicate that dominant emissions are located outside the confined region of plasma, which consists of stochastic magnetic fields with three-dimensional structure intrinsically formed by helical coils. The magnetic field structure in the peripheral region of LHD has been studied experimentally and numerically [11, 12]. In such regions the confinement characteristics of electrons are strongly dependent on their velocity pitch angle with respect to the magnetic field direction. Owing to helical ripple nature of the magnetic field in LHD, electrons move under the influence of a mirror effect. Electrons having a small pitch angle with respect to the magnetic field direction are known as passing electrons, while those with a large pitch angle are known as trapped electrons. Due to the mirror effect, passing electrons can escape easily from the magnetic mirror but trapped electrons are trapped inside ripples of the magnetic field strength. Hence, the confinement characteristics of passing electrons and trapped electrons

are different. Because of very long connection length of the chaotic field-line layer and the mirror confinement effect, low temperature ambient plasma is always present in the LHD chaotic field-line layer located outside the last closed flux surface (LCFS). This ambient plasma outside LCFS is found to be advantageous in achieving high performance plasma confinement in the LHD. Because of very long connection length of lines of force, the ambient plasma helps in reducing heat load to the divertor plate without losing high performance of the core plasma confinement. This plasma provides stabilization effect against MHD instabilities and also suppresses cooling of the core plasma due to charge exchange processes [11]

2. Experimental setup

The Large Helical Device (LHD) is a heliotron type magnetic confinement fusion experimental device with a major radius of 3.6 m and a minor radius of 0.64 m in the standard configuration. Polarization-resolved measurements of the hydrogen Lyman-α line at 121.57 nm from the edge LHD plasma have been realized by incorporating the optical components designed and developed by the CLASP (Chromospheric Lyman-Alpha Spectro-Polarimeter) [13] team into an existing normal incidence VUV spectrometer. Figure 1 provides a schematic drawing of side view of the polarization measurement system with horizontally-elongated poloidal cross-section of LHD. The field of view of the present observation is indicated with dashed lines in Fig. 1.

The polarization measurement system on LHD consists of a normal incidence VUV spectrometer (McPherson model 2253) [14, 15] with a CCD detector and additionally installed optical components, namely, a half-waveplate, a

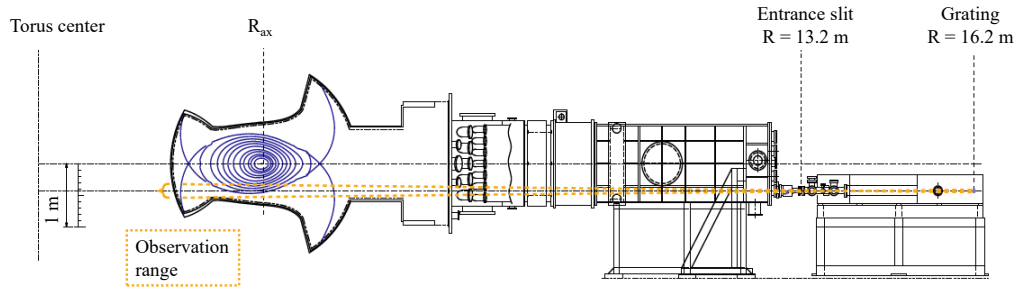

Figure 1: Side view of the polarization measurement system on LHD with the poloidal cross section at horizontally-elongated plasma position in LHD

polarization analyzer, and a high-reflectivity mirror. The schematic representation of arrangement of optical components inside the spectrometer is shown in Fig. 2. The focal length of the spectrometer is 3 m and the working wavelength

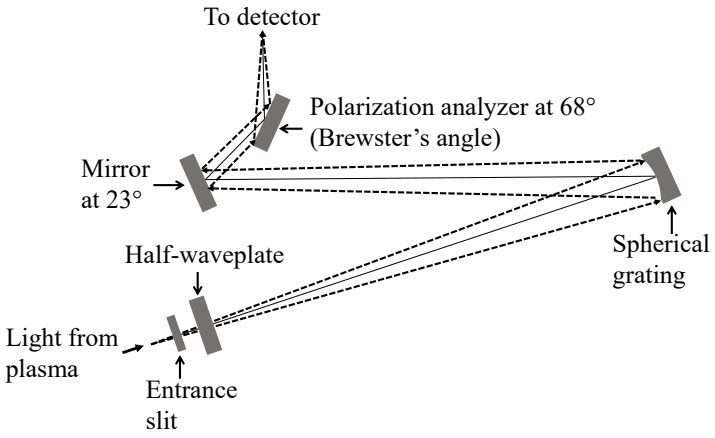

Figure 2: Schematic representation of the arrangement of optical components inside the spectrometer.

range is from 30 nm to 320 nm. This spectrometer is equipped with two spherical gratings of size 65 mm × 150 mm, which are blazed at wavelength

140 nm and 300 nm. The radius of curvature of both gratings is 2.9983 m. The present measurements have been conducted using the grating blazed at 140 nm. A back-illuminated CCD detector, Andor model DV435 with 1024 × 1024 pixels, is used to record spectra. The CCD is generally operated at −20°C to reduce the thermal noise. The size of the CCD is 13.3 mm × 13.3 mm with pixel size 13 μm × 13 μm.

2.1. Working of optical components

2.1.1. Polarization analyzer

Diffracted light beam from the grating includes both p-polarized and s-polarized light. The light with electric vector perpendicular to the plane of incidence is called s-polarized light and the light with electric vector parallel to the plane of incidence is called p-polarized light. The main purpose of using polarization analyzer is to extract one linear polarization component from an incident light by the Brewster's angle reflection. The Brewster's angle, denoted as θ_{B}, can be obtained using the following relation:

$$\tan\theta_{\mathrm{B}} = \frac{n_2}{n_1},$$

where n_1 and n_2 are refractive indices of the medium through which the light travels and of the medium by which the light is reflected, respectively.

The polarization analyzer used for the present measurements consists of thin two-layer coatings of SiO_2 and MgF_2 on a fused silica substrate [16]. This kind of high reflectivity polarizing coating offers high reflectivity for s-polarized light and almost zero reflectivity for p-polarized light at Lyman-α wavelength when used at its Brewster's angle [17]. The Brewster's angle for the polarization analyzer is measured to be 68° and the polarizing power,

defined as

$$P_{\text{power}} = \frac{R_{\text{s}} - R_{\text{p}}}{R_{\text{s}} + R_{\text{p}}},$$

is approximately 0.99 [16], where R_{s} and R_{p} are the reflectivity of s-polarized and p-polarized light, respectively. This result indicates that the light reflected from the analyzer mainly consists of s-polarized component of incident light. Consequently, the polarization analyzer is placed at 68° from the light beam coming from the mirror in the present system. Thus, only the s-polarized component of light observed by spectrometer is monitored at the CCD detector.

2.1.2. High-reflectivity mirror

Since the polarization analyzer must be used at its Brewster's angle, 68°, an optical component is required through which the diffracted light coming from the grating is directed to the polarization analyzer in such a way that the incidence angle is 68°. To meet this requirement, the high-reflectivity mirror is placed at 23° with respect to the diffracted light beam coming from grating. The reflected light beam from the mirror is incident on polarization analyzer with 68° incidence angle. The high-reflectivity mirror is fabricated with Al base coating and MgF_2 overcoating on a CLEARCERAM-Z substrate and has a reflectivity of around 80% for both p-polarized and s-polarized light at 121.57 nm [16]. Although bare Aluminum offers a quite high reflectivity in the VUV range, 84% at 121.57 nm, when exposed to air it can easily become oxidized, and the formed oxidation layer significantly absorbs VUV light. On the other hand, it was demonstrated by Canfield et al. [18] that the use of MgF_2 overlayer coating effectively protects Al against oxidation. Hence, the MgF_2 overlayer coating has been applied on Al, and this form of coating assists in achieving high throughput for the mirror.

2.1.3. Half-waveplate

With the polarization analyzer mentioned above, this system can observe the vertical component of linearly polarized light in the plasma. In order to make the system capable of observing other angle components of linearly polarized light, a half-waveplate dedicated for the Lyman-α wavelength has been incorporated into the system. Here we define the angle of the observed linearly polarized light as "polarization angle", which is denoted as α, and it is measured in clockwise direction as observed from the grating with reference to the vertical axis.

The half-waveplate used in present experiments is made of MgF_2 because MgF_2 offers a high transparency at ultraviolet wavelength and also it is a uniaxial birefringent crystal, i.e., the refractive index of a material depends on polarization and propagation direction of light. The crystal has a single direction governing the optical anisotropy, known as the "optic axis" of crystal. A half-waveplate is fabricated such that the optic axis of the crystal is parallel to the waveplate surface. This results in two axes in the half-waveplate: the ordinary axis, with n_{o} refractive index, and the extraordinary axis, with n_{e} refractive index. The extraordinary axis is parallel to the optic axis of the crystal, whereas the ordinary axis is perpendicular to the optic axis of the crystal. In the case of MgF_2 $n_{\mathrm{o}} < n_{\mathrm{e}}$, hence for simplicity, the ordinary axis and the extraordinary axis are also referred to as the fast axis and the slow axis, respectively. The birefringence is often quantified as the difference between refractive indices n_{e} and n_{o}, i.e., $n_{\mathrm{e}} - n_{\mathrm{o}}$.

The working principle of a half-waveplate is explained by a schematic drawing in Fig. 3. Suppose a plane-polarized wave is normally incident on

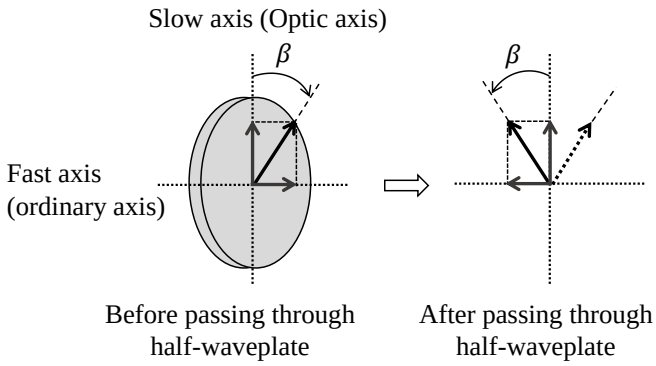

Figure 3: Working principle of a half-waveplate.

a half-waveplate, and the plane of polarization is at an angle β with respect to the slow axis (i.e., optic axis). The incident wave can be decomposed into components polarized along the fast axis and the slow axis. The component polarized along the fast axis travels with a speed $v_{\rm o} = {\rm c}/n_{\rm o}$, while the component polarized along the slow axis travels with a speed $v_{\rm e} = {\rm c}/n_{\rm e}$. As a result, the component polarized along the slow axis is retarded by one half-wave, i.e., by 180° in phase after passing through the half-waveplate. This describes a plane-polarized wave, but makes an angle η on the other side of the slow axis as shown in Fig. 3. Thus, the original wave has been rotated by an angle 2η.

The half-waveplate used in the present measurement is a compound zero-order waveplate consisting of two stacked MgF_2 plates with slightly different thicknesses and their optic axes are rotated by 90° with respect to each other. The phase retardation, δ, introduced by such a waveplate with a thickness difference of $d_1 - d_2$ is given by

$$\delta = 2\pi \frac{(n_{\rm e} - n_{\rm o})(d_1 - d_2)}{\lambda},$$

where, $n_e - n_o$ is the birefringence at wavelength λ. From the measurements carried out by the CLASP team, it was found that $n_e - n_o = 0.00419 \pm 0.00004$ at 121.57 nm and the waveplate with a thickness difference of 14.51 μm works as a half-waveplate at the Lyman-α wavelength [19].

In the present experiment, the half-waveplate is placed just behind the entrance slit, and the half-waveplate is continuously rotated in the clockwise direction as observed from the grating during the measurement. The angle of half-waveplate optic axis, denoted here as θ, is measured in the clockwise direction with respect to the vertical axis. In the following discussion the term "optic axis" is used to express the optic axis of the plate on which light wave is first incident. The incident light coming from the LHD plasma can be regarded to have linearly polarized light components at all directions. When the optic axis angle is θ, the linearly polarized light at an angle 2θ is rendered to be vertical after passing through the half-waveplate as shown in Fig. 4, and is subsequently detected. In this way, by using the combination of

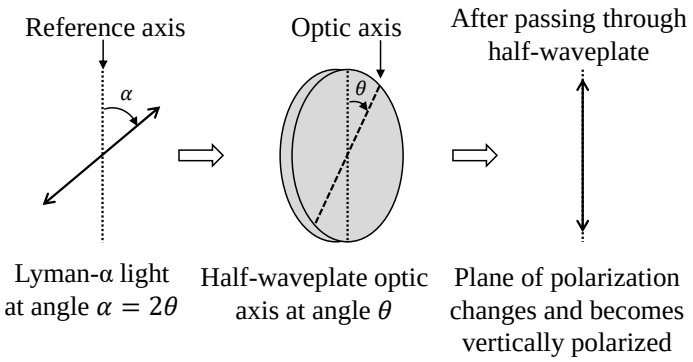

Figure 4: Half-waveplate changes the plane of polarization.

a rotating half-waveplate and a polarization analyzer, the spectra of linearly

polarized Lyman-α light at all angles are obtained sequentially.

During the measurement, the cycle time of Lyman-α line spectral observation is 50 ms with an exposure time of 16 ms, and the period of the half-waveplate rotation is 0.8 s. Under such conditions, linearly polarized light at every 45° angle is monitored. Since the detector always receives vertical (s-polarized) component of light, final measurements are not affected by different grating efficiency values for p-polarized and s-polarized light. The system is also capable of acquiring spectra with better angular resolution, i.e., with smaller step size of angle, by increasing the half-waveplate rotation period. Depending on the steady-state phase duration of the discharge, the period of the half-waveplate rotation is determined.

2.2. Viewing geometry of the spectrometer

In this paper we focus on the LHD discharge with shot no. 138800, which is an electron cyclotron heated (ECH) discharge. For this discharge the magnetic axis is at $R_{\mathrm{ax}} = 3.75\,\mathrm{m}$ and the magnetic field strength is 2.64 T at the magnetic axis. Figure 5 shows the schematic drawing of the poloidal cross-section at horizontally-elongated plasma position of LHD with the magnetic surfaces for the present magnetic field configuration. The variables Z and R represent vertical and radial coordinates, respectively. The observation range of the spectrometer is approximately 0.15 m wide in Z coordinate. $Z = -0.4\,\mathrm{m}$ location can be considered as a main line-of-sight and it is shown by a dashed line. In the LHD, divertor plates made of graphite are placed at the line-of-sight end which is terminating at the vacuum chamber surface, so the reflection of light is expected to be very small and the observed light contains negligible reflected light.

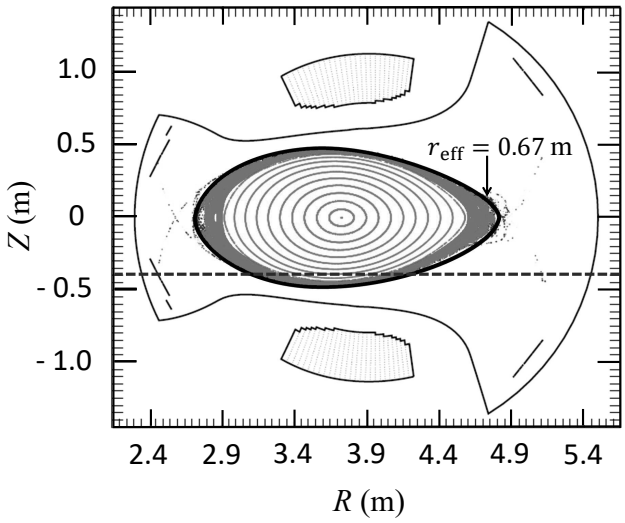

Figure 5: Schematic drawing of poloidal cross section at horizontally-elongated plasma of LHD with the magnetic surfaces for the magnetic axis at $R_{\rm ax} = 3.75\,{\rm m}$. The line-of-sight of the spectrometer is indicated by a dashed line. The magnetic surface with $r_{\rm eff} = 0.67\,{\rm m}$ is also shown.

The previous studies on the hydrogen line emission from the LHD plasma suggest that the dominant hydrogen emission locations can be approximated to be at $r_{\rm eff} = 0.67\,{\rm m}$ [9, 10] where $r_{\rm eff}$ is the effective minor radius of the plasma. From this result, it is inferred that on the spectrometer line-of-sight, the Lyman-α line is emitted at both the inboard side and the outboard side of the device, and intensity observed by the spectrometer is the sum of these intensities.

3. Results and discussion

The main parameters of the discharge, i.e., stored energy ($W_{\rm P}$ in kJ), total ECH power (in MW), electron temperature at magnetic axis (T_{e0} in

keV), line averaged electron density ($\bar{n}_e$ in m^{-3}), and H_α signal (in arbitrary units) obtained with a photomultiplier tube based system, are shown in Fig. 6.

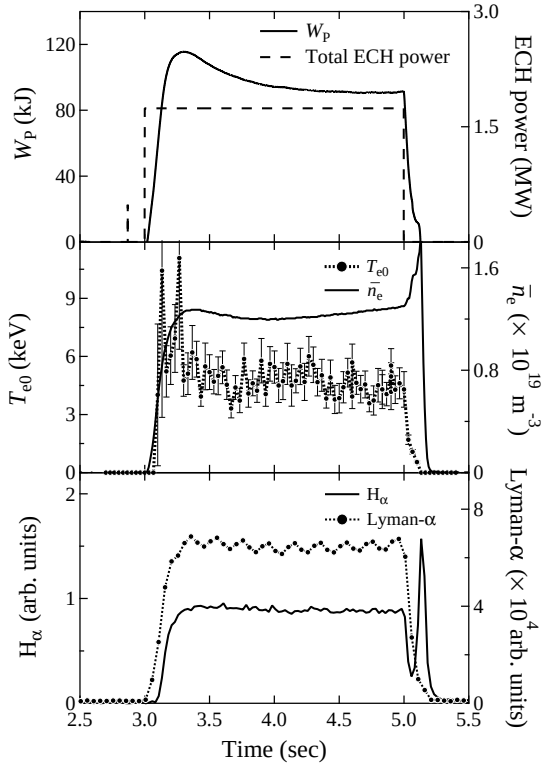

Figure 6: Main parameters of shot no. 138800: (a) stored energy (W_p in kJ) and total ECH power (in MW) (b) electron temperature at magnetic axis ($T_{\mathrm{e}0}$ in keV) and line averaged electron density ($\bar{n}_\mathrm{e}$ in m^{-3}) (c) H_α signal acquired using a photomultiplier tube based system (in arbitrary units) and Lyman-α line obtained for the present measurement (in arbitrary units).

3.1. Polarization degree

As discussed in Sec. 2.1.3, spectra of linearly polarized Lyman-α light from the edge LHD plasma have been acquired at every 45° angle with the polarization measurement system. An example of a spectrum acquired during the steady-state time period of the discharge is shown in Fig. 7, where both the hydrogen and the deuterium lines can be seen. The intensity integrated

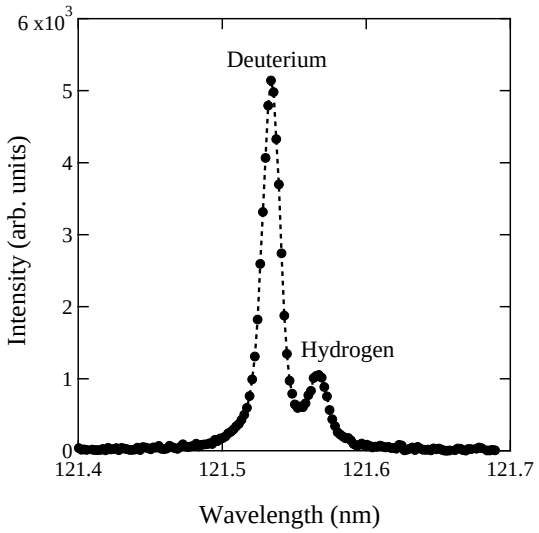

Figure 7: Typical background subtracted spectrum at 121.56 nm obtained during steady-state phase of an LHD discharge showing hydrogen and deuterium peaks.

over the entire wavelength range shown in Fig. 7 for each time frame has been calculated, and the result is plotted as a function of time, t, with circles in Fig. 6 (c) along with H_α signal.

In Fig. 8 the experimentally measured intensity and polarization angle are plotted as a function of time. The experimental intensity shows a modulation, which is synchronized with a half-waveplate rotation period. This result

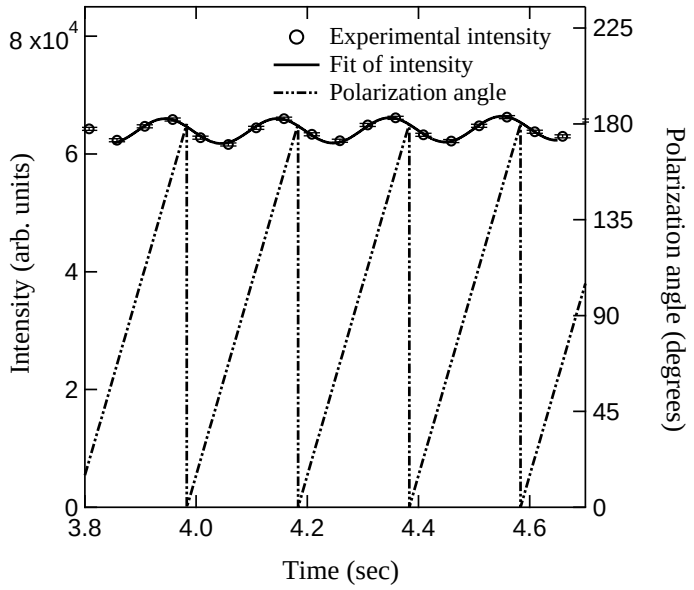

Figure 8: Temporal profile of Lyman-α line is shown with open circles and solid line represents the fitted curve. The polarization angle is shown with a dash-dotted line.

clearly indicates that the observed Lyman-α line is polarized. Since the light intensities at polarization angles α and $180^\circ+\alpha$ are not distinguishable, as can be seen from Fig. 4, the intensity profile is the same for polarization angles from 0° to 180° and from 180° to 360°. Due to this fact the polarization angle is plotted only in the range from 0° to 180° in Fig. 8.

For evaluating the polarization degree, steady-state time phase of the discharge, i.e., from $t = 3.85\,\mathrm{s}$ to $t = 4.65\,\mathrm{s}$, is considered so that it can be assumed that the polarization state is not changed during this time period. This time duration with $\Delta t = 0.8\,\mathrm{s}$ corresponds to one complete rotation of

the half-waveplate. In the present case we define the polarization degree as

$$P = \frac{I_{\max} - I_{\min}}{I_{\max} + I_{\min}}, \tag{1}$$

where $I_{\min}$ and $I_{\max}$ are the minimum and maximum intensities in the temporal profile, respectively.

The least-squares fitting is performed on temporal variation of the intensity, $I(t)$, with a function

$$I(t) = f(t)[1 + P\sin(\omega t + \theta)], \tag{2}$$

where $f(t)$ represents the global intensity variation, which is here expressed by a second order polynomial, P is magnitude of polarization degree, and θ is the phase offset. In the present case $\omega = 10\,\pi$. To perform fitting of temporal variation, the profile is first fitted with $f(t)$ and then parameters derived for $f(t)$ are used as the initial guess for the final fitting to obtain accurate fitting results.

As a result of fitting, $P = 0.033$ is obtained. The fitting result is shown with a solid line in Fig. 8. The error in measured intensity is very small and actual uncertainty in the present measurement is mainly due to unsteadiness of the discharge which is recognized as a discrepancy of the measured intensities from the fitted curve in Fig. 8. The root mean squared error of measured intensity with respect to fitted curve is evaluated and given as error bars in Fig. 8. By using the value of uncertainty in measured intensities, the value of polarization degree $P = 0.033 \pm 0.004$.

3.2. Polarization angle

The variation of intensity with α is shown in Fig. 9 for the time duration from $t = 3.98\,\mathrm{s}$ to $t = 4.18\,\mathrm{s}$. The angle α is varying from 0° to 180° in

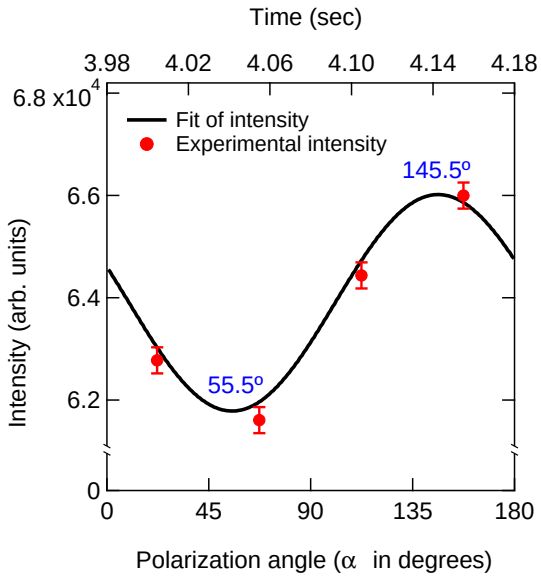

Figure 9: Plot of Lyman-α intensity vs. polarization angle, α. Points show experimental intensity and the fit of intensity is shown with a solid line.

this duration. This plot indicates that minimum and maximum intensities are observed at $\alpha = 55.5°$ and $\alpha = 145.5°$, respectively. Here we consider the meaning of the angles at minimum and maximum intensity. Since the anisotropy in EVDF is thought to be related to the magnetic field, these angles are also expected to have some relation with the magnetic field.

There are two possible emission locations of Lyman-α on the present line-of-sight as mentioned above and directions of the magnetic field are known at these locations. Figure 10 illustrates the schematic representation of the magnetic field directions on the line-of-sight. $\boldsymbol{B}_{\mathbf{i}}$ and $\boldsymbol{B}_{\mathbf{o}}$ represents magnetic field vectors at the inboard and the outboard side, respectively. The angle of projection of the magnetic field on the plane perpendicular to

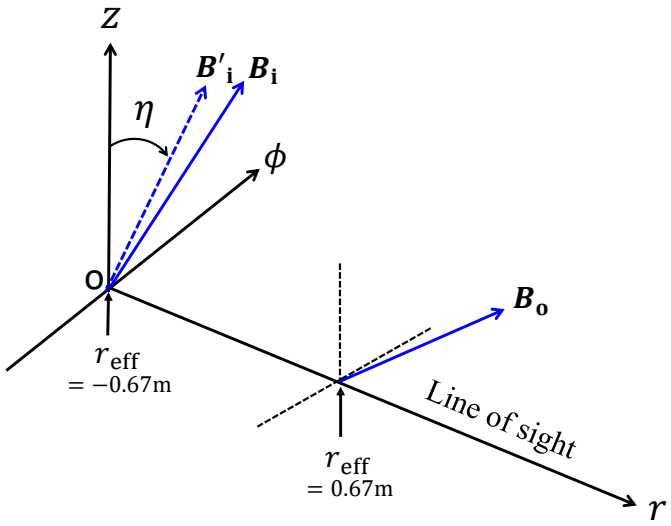

Figure 10: Schematic representation of magnetic field directions on line-of-sight. $\boldsymbol{B}_\mathbf{i}$ and $\boldsymbol{B}_\mathbf{o}$ represent magnetic field vectors at the inboard and the outboard side, respectively. $\boldsymbol{B}'_\mathbf{i}$ indicates the projection of $\boldsymbol{B}_\mathbf{i}$ on the $z-\phi$ plane.

the line-of-sight, $z-\phi$ plane, with respect to z axis is calculated at each emission location. Here we express this angle with η. The value of η is found to be 56.1° and 108.5° at the inboard side and the outboard side, respectively. It is apparent that the angle η at the inboard side, 56.1°, is approximately coinciding with the angle at minimum intensity, 55.5°. In other words, the observed intensity is minimum in the direction parallel to $\boldsymbol{B}_\mathbf{i}$ and it is maximum in the direction perpendicular to $\boldsymbol{B}_\mathbf{i}$. This result suggests that the polarized emission is mainly coming from the inboard side plasma and, therefore, the observed polarization in the Lyman-α line is mainly caused by anisotropic EVDF at the inboard side plasma.

The preliminary results of a simulation model code [20, 21] show that

the observed behavior of intensity, i.e., minimum intensity in the direction parallel to the magnetic field and maximum intensity in the direction perpendicular to the magnetic field, indicates that the value of polarization degree is negative. According to model results, negative polarization degree implies that electron temperature in the perpendicular direction to the magnetic field is higher than that in the parallel direction.

In summary, we have clearly observed polarization of the order of 0.033 in Lyman-α line. For the present measurement, final value of polarization degree is -0.033 ± 0.004. We have tried to fit the hydrogen and deuterium lines individually and have obtained nearly the same results regarding the polarization degree and polarization angle. Therefore, we can regard these two species as identical in the present analysis and consider only the entire intensity from the two lines. It has been confirmed that under the same plasma conditions, polarization degree and angle are reproducible.

It is strongly suggested that the observed polarization is mainly caused at the inboard side out of the two possible emission locations on the line-of-sight. A possible reason for polarized emission originating at the inboard side is that the line emissions observed are dominated by those at the inboard side. The neutral flux generally has a poloidal asymmetry in the LHD following an inhomogeneous divertor flux, and therefore an asymmetry in the poloidal neutral flux distribution is expected [22]. It is also possible that even though the anisotropy is smaller at the outboard side, line emissions at the outboard side significantly contribute to the observed line intensity. In that case the polarization degree at the inboard side can be larger than that derived in this paper. There is actually some difference regarding the connection length

structure between in the inboard side and in the outboard side [23], and this could cause different states in the anisotropic EVDF in these regions. However, a more detailed investigation is necessary to deduce a conclusive statement.

Acknowledgements

The authors are grateful to the CLASP team for providing optical components for the LHD experiments. The authors also thankfully acknowledge support of the LHD Experiment Group and the technical staff of LHD for carrying out experiments in LHD. This work is partly supported by JSPS KAKENHI Grant Number 26287148 and by the National Institute for Fusion Science grant administrative budget (ULHH028).

References

[1] Hiroshi Aikawa. The measurement of the anisotropy of electron distribution function of a magnetized plasma. *Journal of the Physical Society of Japan*, 40(6):1741–1749, 1976.

[2] Taiichi Shikama, Shinichiro Kado, Shin Kajita, and Satoru Tanaka. The effect of superthermal electrons on mach probe diagnostics. *Japanese journal of applied physics*, 43(2R):809, 2004.

[3] RL Stenzel, W Gekelman, N Wild, JM Urrutia, and D Whelan. Directional velocity analyzer for measuring electron distribution functions in plasmas. *Review of Scientific Instruments*, 54(10):1302–1310, 1983.

[4] MD Bowden, T Okamoto, F Kimura, H Muta, Kiichiro Uchino, K Muraoka, T Sakoda, M Maeda, Y Manabe, M Kitagawa, et al. Thomson scattering measurements of electron temperature and density in an electron cyclotron resonance plasma. *Journal of applied physics*, 73(6):2732–2738, 1993.

[5] E Yatsuka, T Hatae, and Y Kusama. Principles for local measurement of anisotropic electron temperature of plasma using incoherent Thomson scattering. *Nuclear Fusion*, 51(12):123004, 2011.

[6] F Skiff, DA Boyd, and JA Colborn. Measurements of electron parallel-momentum distributions using cyclotron wave transmission. *Physics of Fluids B: Plasma Physics*, 5(7):2445–2450, 1993.

[7] DJ Thuecks, F Skiff, and CA Kletzing. Measurements of parallel electron velocity distributions using whistler wave absorption. *Review of Scientific Instruments*, 83(8):083503, 2012.

[8] Takashi Fujimoto and Atsushi Iwamae. *Plasma Polarization Spectroscopy*. Springer, 2008.

[9] Atsushi Iwamae, Masayuki Hayakawa, Makoto Atake, Takashi Fujimoto, Motoshi Goto, and Shigeru Morita. Polarization resolved H α spectra from the large helical device: Emission location, temperature, and inward flux of neutral hydrogen. *Physics of plasmas*, 12(4):042501, 2005.

[10] Atsushi Iwamae, Atsushi Sakaue, Nobuhiro Neshi, Jun Yanagibayashi, Masahiro Hasuo, Motoshi Goto, and Shigeru Morita. Hydrogen emission location, temperature and inward velocity in the peripheral helical

plasma as observed with plasma polarization spectroscopy. *Journal of Physics B: Atomic, Molecular and Optical Physics*, 43(14):144019, 2010.

[11] T Watanabe, Y Matsumoto, M Hishiki, S Oikawa, H Hojo, M Shoji, S Masuzaki, R Kumazawa, K Saito, T Seki, et al. Magnetic field structure and confinement of energetic particles in the LHD. *Nuclear fusion*, 46(2):291, 2006.

[12] Yutaka Matsumoto, Shun-ichi Oikawa, and Tsuguhiro Watanabe. Field line and particle orbit analysis in the periphery of the Large Helical Device. *Journal of the Physical Society of Japan*, 71(7):1684–1693, 2002.

[13] R Kano, J Trujillo Bueno, A Winebarger, F Auchère, N Narukage, R Ishikawa, K Kobayashi, T Bando, Y Katsukawa, M Kubo, et al. Discovery of scattering polarization in the Hydrogen Lyα line of the solar disk radiation. *The Astrophysical Journal Letters*, 839(1):L10, 2017.

[14] Shigeru Morita and Motoshi Goto. Space-resolved vuv spectroscopy using the 3 m normal incidence spectrometer with back-illuminated CCD detector in the LHD. *Review of scientific instruments*, 74(3):2036–2039, 2003.

[15] Tetsutarou Oishi, Shigeru Morita, Chunfeng Dong, Erhui Wang, Xianli Huang, Motoshi Goto, LHD Experiment Group, et al. Space-resolved 3 m normal incidence spectrometer for edge impurity diagnostics in the large helical device. *Applied optics*, 53(29):6900–6912, 2014.

[16] Noriyuki Narukage, Masahito Kubo, Ryohko Ishikawa, Shin-nosuke Ishikawa, Yukio Katsukawa, Toshihiko Kobiki, Gabriel Giono, Ryouhei

Kano, Takamasa Bando, Saku Tsuneta, et al. High-reflectivity coatings for a vacuum ultraviolet spectropolarimeter. *Solar Physics*, 292(3):40, 2017.

[17] Françoise Bridou, Mireille Cuniot-Ponsard, J-M Desvignes, Alexander Gottwald, Udo Kroth, and Mathias Richter. Polarizing and non-polarizing mirrors for the hydrogen Lyman-α radiation at 121.6 nm. *Applied Physics A*, 102(3):641–649, 2011.

[18] LR Canfield, G Hass, and JE Waylonis. Further studies on MgF_2-overcoated aluminum mirrors with highest reflectance in the vacuum ultraviolet. *Applied optics*, 5(1):45–50, 1966.

[19] Ryohko Ishikawa, Ryouhei Kano, Takamasa Bando, Yoshinori Suematsu, Shin-nosuke Ishikawa, Masahito Kubo, Noriyuki Narukage, Hirohisa Hara, Saku Tsuneta, Hiroko Watanabe, et al. Birefringence of magnesium fluoride in the vacuum ultraviolet and application to a half-waveplate. *Applied optics*, 52(34):8205–8211, 2013.

[20] M Goto and N Ramaiya. Modeling of Lyman-α line polarization in fusion plasma due to anisotropic electron collisions. In *Journal of Physics: Conference Series*, volume 1289, page 012011. IOP Publishing, 2019.

[21] Nilam RAMAIYA, Motoshi GOTO, Tetsutarou OISHI, and Shigeru MORITA. Study of Lyman-α Polarization due to Anisotropic Electron Collisions in LHD. *Plasma and Fusion Research*, 14:3402083–3402083, 2019.

[22] M Goto and S Morita. Determination of the line emission locations in a large helical device on the basis of the Zeeman effect. *Physical Review E*, 65(2):026401, 2002.

[23] Suguru Masuzaki, T Morisaki, N Ohyabu, A Komori, H Suzuki, N Noda, Y Kubota, R Sakamoto, K Narihara, K Kawahata, et al. The divertor plasma characteristics in the Large Helical Device. *Nuclear fusion*, 42(6):750, 2002.